Microelectronics Journal 38 (2007) 285–298

Microelectronics Journal

www.elsevier.com/locate/mejo

Dynamic power density, wavelength, and switching time modulation of optically triggered power transistor (OTPT) performance parameters ☆

Tirthajyoti Sarkar, Sudip K. Mazumder*

Laboratory for Energy and Switching-electronics Systems (LESES), Department of Electrical and Computer Engineering, University of Illinois at Chicago, 851 S. Morgan Street, M/C: 154, 1020 SEO, Chicago, IL 60607, USA

Received 2 September 2006; accepted 22 November 2006

Abstract

Optical modulation by varying the intensity, wavelength, or switching time can dynamically alter the performance parameters of direct optically controlled power semiconductor device. Understanding the effect of optical parameters on these parameters from a first principle approach is necessary for making optimal design choices and gaining design insights. We focus on performance parameters whose variations with direct optical modulation have not been reported previously for a power semiconductor such as switching times and on-state resistance. We carry out analytical modeling and two-dimensional (2D) finite-element simulations for a GaAs/AlGaAs based superjunction lateral optically controlled power transistor that has been fabricated and successfully tested for high-voltage capability. It is shown that optical power density can modulate on-state resistance and more importantly the trade-off curve between breakdown voltage and on-state resistance. A closed-form analytical equation relating switching times with optical parameters via logarithmic function is derived and the nonlinear variation of on-state resistance and switching time with optical wavelength is illustrated. We also derive the analytical expression for power device rise time as a function of optical signal rise time and show that they are related by Lambert's *W*-function with exponential coefficients.

Keywords: Optical modulation; Power semiconductor; GaAs/AlGaAs; Wavelength; Switching; Analytical modeling

1. Introduction

In an environment where external radio-frequency (RF) signals can interact with power electronics, for example *fly-by-light* (FBL) architecture for next-generation avionics, electromagnetic interference (EMI) is a critical issue [1]. Recent research by US Air force [2,3] has shown that tangible reductions in weight, volume, and cost are possible through the application of emerging photonic technologies for vehicular power-management systems by elimination of EM shielding around copper wiring, which is replaced by lightweight optical fiber. In this respect, next-generation photonic power-electronic systems (as shown in Fig. 1a), based on optically triggered devices (OTDs) [4–6] provide key advantages over conventional electrically triggered device (ETD) based switching power electronics (as shown in Fig. 1b). Prospective applications for such OTDs include power management systems in military and commercial aircrafts, spacecrafts, electric warships, naval planes and helicopters, battle tanks, armored cars, field artillery vehicles. Moreover, as can be seen from Fig. 1, such device is triggered directly by light and therefore does not need a voltage differential between source and gate (necessitating separate high- and low-side drivers for multilevel converters) like most widely used power devices, i.e. MOSFET or IGBT.

Direct optically controlled power device is the first major step towards photonic power-electronic systems. Most

☆ *Patent disclaimer:* The work described in this paper, including the subsections and the figures therein, are protected by the following provisional patent filed by the University of Illinois at Chicago: S.K. Mazumder and T. Sarkar, "Optically-triggered power system and devices", USPTO Provisional Patent, Filing # CY083, September 2005. The PCT application has been filed in June of 2006.

*Corresponding author. Tel.: +1 312 355 1315; fax: +1 312 996 6465.
E-mail address: mazumder@ece.uic.edu (S.K. Mazumder).

0026-2692/$ - see front matter © 2007 Published by Elsevier Ltd.
doi:10.1016/j.mejo.2006.11.020

Nomenclature

h	Planck's constant;	τ_a	ambipolar lifetime
$\hbar$	reduced Planck's constant, i.e. $(h/2\pi)$	τ_{nH}	high-level injection electron lifetime
c	velocity of electromagnetic wave	τ_{nL}	low-level injection electron lifetime
k	Boltzmann constant	η	quantum efficiency
T	absolute temperature	R	surface reflectivity
n, p	electron, hole carrier densities	P	optical power density
q	electronic charge	λ	wavelength of the optical beam
E	electric field	α	optical absorption coefficient
G_n, G_p	electron, hole generation rates	C_d	radiative recombination coefficient
G_{opt}	spatially averaged photogeneration rate	L_{body}	length of the P-body region
μ_a	ambipolar mobility	L_{drift}	drift region length
D_a	ambipolar diffusion constant	t_r	OTPT rise time
		t_0	optical signal rise time

desirable properties of such a device would be: (1) high optical and electrical triggering gain; (2) non-latched turn-on and turn-off controllabilities with a single optical monochromatic source; and (3) optical fiber coupling. Moreover, basic electrical properties like high breakdown voltage, fast switching times, and low on-state resistance need to be met.

This class of devices includes bulk photoconductive switches (PCS), bistable optically controlled switches (BOSS), optothyristor, light-triggered thyristor (LTT), and static induction phototransistor (SIPT), for which a comprehensive review can be found in [6,7] and references therein. Although many issues related to device modeling, design, fabrication, and characterization have been researched, no specific study has been reported on the optical modulation capabilities of this class of device from power semiconductor device performance point of view.

Use of optical modulation techniques for power semiconductors have primarily been applied for measurement, reliability analysis, and characterization techniques [8,9] but not as means of dynamically altering device performance parameters. On the other hand, research on optical modulation and control of other conventional electrical devices like MOSFET [10,11], MESFET [12–14], or HEMT [15] have primarily concentrated on microwave systems, low-power signal detection, and optical communication applications which have different requirements from power semiconductor devices and associated power electronics applications. The common feature of these works is that optical signal was applied to modulate steady-state properties such as I–V characteristic [10,11,13], RC time constant [14], RF s-parameters [12], or pinch-off voltage [15] which are very important from the corresponding application area point of view but do not cover the direct modulation aspects of switching properties like rise and fall time, which are important in power electronics applications. Moreover, modulations are reported mainly with respect to the power of the optical signal and not on

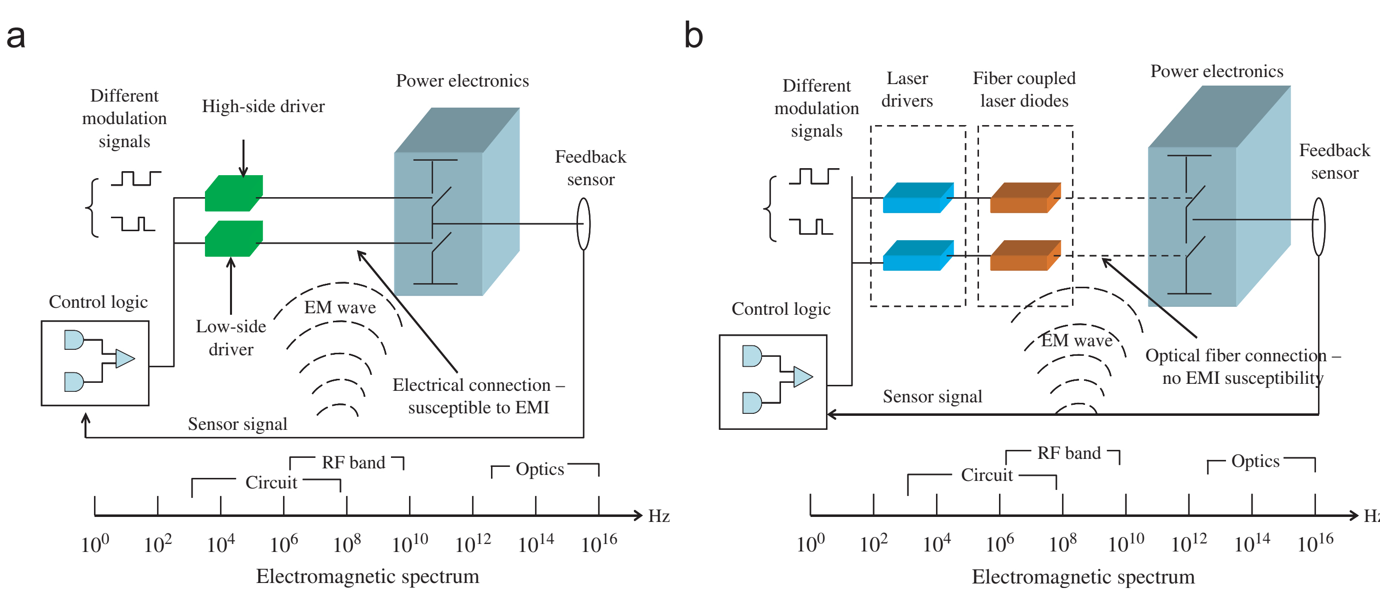

Fig. 1. Effect of EMI on power electronics system based on (a) ETD and (b) OTD.

optical wavelength. For fast switching direct optically controlled power semiconductors, nonlinear variation of reflectivity and optical absorption coefficient with wavelength demands an optimum operating wavelength to be investigated. Wavelength-dependent photogenerated current density and optical power-dependent drain–source current for optically controlled bipolar mode field-effect transistor (BMFET) were reported in [16,17] but an explicit description of the variation of on-state resistance and switching time with varying wavelength or optical power was not given. Also, no study was reported describing how the switching characteristic of BMFET will depend on the switching times of the optical signal. The rise and fall time for a direct optically controlled power device depends on the switching times of corresponding optical triggering signal and a study is required to estimate how the variation in rise time of the triggering optical signal may affect that of the main power device.

Another category of research studies in this particular area deals with electrically gated main power device being indirectly controlled by optical signals. Amplitude, wavelength, and pulse-width modulation strategies for optically triggered power DMOSFET (OT-MOS) were reported in [18] with Si power MOSFET and GaAs photodiode and photoconductive triggering structures. However, the power MOSFET being an electrically gated device, the switching properties of OT-MOS are largely limited by junction and oxide capacitance of the MOSFET and exhibit less dependence on optical parameters than a direct optically controlled device. Similar studies related to the switching times of an optically controlled power bipolar junction transistor (BJT) is reported in [19] using light-emitting diode (LED)–phototransistor pair as the driving circuit. Si phototransistor controlled SiC Darlington BJT has been proposed [20] for FBL applications but not much details on the optical modulation is provided.

Direct optically triggered power transistor (OTPT) [4], based on GaAs/AlGaAs heterojunction structure, has been reported recently illustrating the basic operating principle, experimentally verified high-voltage breakdown capability and fabrication details. In this paper, we illustrate how by varying power density, wavelength, and switching times of the triggering optical signal, the performance parameters of the OTPT can be modulated. We focus on those parameters whose variations with direct optical modulation have not been reported previously for a power semiconductor such as switching times and on-state resistance. We show that breakdown voltage vs. on-state resistance trade-off curve, which is generally independent of triggering parameters for ETDs, can be modulated by optical power density variation. We derive, by solving non-steady-state continuity equation, the analytical relation between OTPT switching times and optical power density. We also derive the analytical expression for OTPT rise time considering a linear ramp-type time-varying optical signal and show that these quantities are inter-related by a Lambert's *W*-function with exponential coefficients. Analytical modeling was done to gain important insights about the choice of optical triggering parameters and device design procedure. Two-dimensional (2D) finite-element simulations were done to verify the predictions from the analytical models about the variation of device parameters with optical modulation.

2. OTPT structure and principle of operation

We show in Fig. 2, the structural schematic of the OTPT. It has a lateral structure with two electrodes—source and drain. The optical window is defined by the anti-reflecting layer between the electrodes. The bottom P-type AlGaAs layer acts as the charge-compensating layer and the doping and thickness values of the epitaxial layers, that is d_1, d_2, N_1, N_2, d_{cap}, and N_{cap}, have been designed such as to realize the superjunction charge-balance [4], i.e., the total positive charge contributed by P-AlGaAs layer nullifies the total negative charge contributed by the top N-type layers. The OTPT structure features a deep-implanted P-body which extends all the way up to the P-AlGaAs layer. The junction between the P-body and the N-drift region results in almost ideal parallel-plate like electric field distribution during blocking state. Wider bandgap AlGaAs surface barrier layer is used to suppress Fermi-pinning and surface recombination velocity effects, which may degrade the overall device performance by lowering the optical triggering efficiency significantly and increasing on-state resistance.

In the blocking or open state, the applied voltage is supported by the reverse biased P–N junction between the P-body and N-drift regions. When triggering light beam falls on the device, in the optical window region it is absorbed and it generates electron–hole plasma by photogeneration. They are mobilized by the local electric field and are attracted by the drain and source electrodes and constitute electron and hole currents thereby closing the switch. If the light beam is sustained the conductivity is sustained too and the switch remains closed. When the

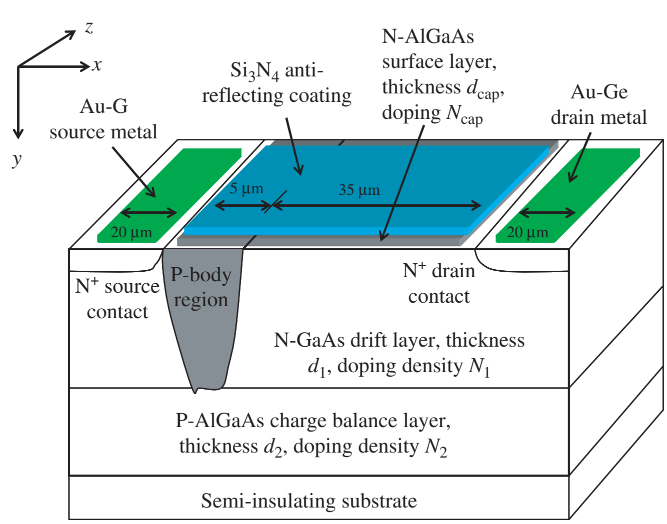

Fig. 2. Structural schematic of the OTPT.

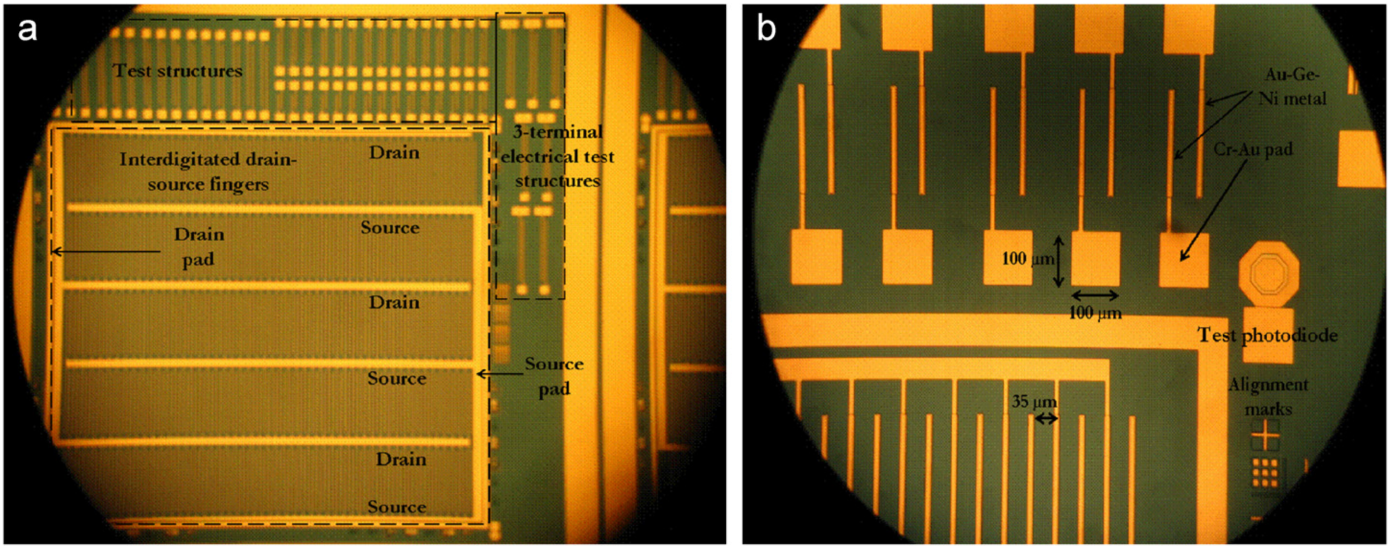

Fig. 3. (a) Overall OTPT micrograph and (b) detailed micrograph showing dimensions and contacts.

light shuts off, the carriers are recombined among themselves and the switch goes back to its high-resistivity blocking state.

Figs. 3a and b show micrographs of a prototype OTPT device. These devices have 1.0 µm thick N-GaAs (doping density $\sim 5.0\times10^{13}\,\mathrm{cm}^{-3}$) layer grown (by metal-organic chemical vapor deposition (MOCVD) technique) on top of 300 nm thick P-$\mathrm{Al_{0.2}Ga_{0.8}As}$ layer (doping density of $3.0\times10^{14}\,\mathrm{cm}^{-3}$). A 100 nm N-AlGaAs layer (doping density $1.45\times10^{15}\,\mathrm{cm}^{-3}$) is grown and patterned for surface passivation. Si implantation at 100 keV energy with $5.0\times10^{14}\,\mathrm{cm}^{-2}$ dose is carried out for N^+ source and drain contact regions. Beryllium implantation at 150 keV and $2.0\times10^{13}\,\mathrm{cm}^{-2}$ dose has been used to create the P-body. Activation of both N- and P-type implants is carried out at a rapid thermal processor (RTP) at 850 °C for 5 min using a GaAs undoped wafer as proximity anneal cap. Plasma-enhanced chemical vapor deposited (PECVD) $\mathrm{Si_3N_4}$ of 100 nm thickness is used as anti-reflective (AR) coating. P-type guard rings are created around individual test structures for reducing electric fields on the edge. Electron beam evaporated Au–Ge alloy (annealed at 400 °C) is used as drain and source contacts and thick Cr–Au metallization is done to form bonding pads.

3. Optical modulations

3.1. On-state resistance and on-state resistance vs. breakdown voltage curve modulated by optical power density

For a given device area, variation of on-state resistance (R_{on}) with breakdown voltage (V_{Br}) in conventional power semiconductor devices approximately follows the power law of the form:

$$R_{\mathrm{on}} \approx \beta V_{\mathrm{Br}}^{\gamma}, \tag{1}$$

where β is a constant and γ is the exponent. A comprehensive review of the different forms of the power law for different classes of devices (with different β and γ) can be found in [21]. Once the device is fabricated with specific dopings and geometry, this curve cannot be easily modulated with triggering properties for ETDs. This is because β does not contain any physical term related to triggering parameters.

For the OTPT, physics-based analyses yield two transcendental equations, which couple V_{Br} and R_{on} through the drift length (L_{drift}). V_{Br} can be estimated from the impact ionization model of GaAs [22]

$$\int_0^{L_{\mathrm{drift}}}\Big[2.994\times10^5\exp\Big(-\big(6.648\times10^5 L_{\mathrm{drift}}/V_{\mathrm{Br}}\big)^{1.6}\Big) +2.215\times10^5\exp\Big(-\big(6.57\times10^5 L_{\mathrm{drift}}/V_{\mathrm{Br}}\big)^{1.75}\Big)\Big]\,\mathrm{d}x = 1. \tag{2}$$

For estimation of R_{on} we need to obtain steady-state carrier concentration by solving continuity equation. Fig. 4 demonstrates that current densities in x-direction are much higher compared to that in y-direction and therefore we focus on one-dimensional (1D) continuity equation whose general form for electron and hole are as follows:

$$\frac{\partial n}{\partial t} = D_{\mathrm{n}}\frac{\partial^2 n}{\partial x^2} + \mu_{\mathrm{n}}E\frac{\partial n}{\partial x} + G - R,$$
$$\frac{\partial p}{\partial t} = D_{\mathrm{p}}\frac{\partial^2 p}{\partial x^2} + \mu_{\mathrm{p}}E\frac{\partial p}{\partial x} + G - R, \tag{3}$$

where E denotes electric field, n, p are electron and hole densities, D_{n}, D_{p} are electron and hole diffusion coefficients, μ_{n}, μ_{p} are electron and hole mobilities, G is the generation rate and R is the total recombination rate. We assume that both Shockley–Read–Hall (SRH) and radiative band-to-band direct recombination occurs in OTPT

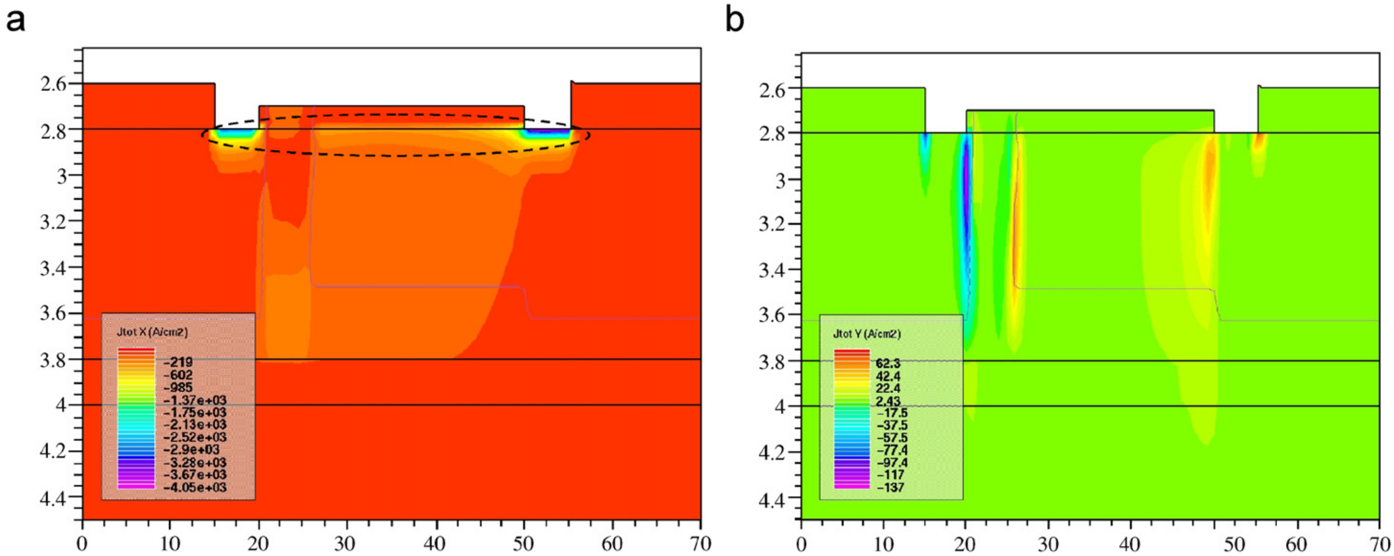

Fig. 4. Total current density (negative value because of majority electron conduction) in the OTPT during conduction state in (a) x-direction and (b) y-direction. The photogenerated channel is indicated by the high current density near the surface in (a).

because of the direct bandgap nature of GaAs. SRH recombination rate is given by [23],

$$R_{\mathrm{n,SRH}} = v_{\mathrm{th}}\sigma_{\mathrm{o}}N_{\mathrm{t}}\frac{pn - n_{\mathrm{i}}^2}{p + n + 2n_{\mathrm{i}}\cos h(E_{\mathrm{t}} - E_{\mathrm{i}}/kT)} = R_{\mathrm{p,SRH}}, \tag{4}$$

where $R_{\mathrm{n,SRH}}$ and $R_{\mathrm{p,SRH}}$ are electron and hole SRH recombination rates, v_{th} is thermal velocity, σ_{o} is common capture cross-section, N_{t} is the trap centre density, E_{t} is the trap energy level, E_{i} is the equilibrium energy level, n_{i} is the intrinsic carrier density, k is the Boltzmann constant and T is the absolute temperature.

For OTPT, typical doping density in the P-body region is $\sim 10^{17}\,\mathrm{cm}^{-3}$ and in the N-drift region is $\sim 10^{14}\,\mathrm{cm}^{-3}$ whereas the GaAs intrinsic carrier density is $2.1\times 10^{6}\,\mathrm{cm}^{-3}$. Clearly, the product $pn \gg n_{\mathrm{i}}^2$ for any region of the device and we can neglect the contribution from the n_{i} related terms. Therefore, SRH recombination rate can be re-written as

$$R_{\mathrm{n,SRH}} = \frac{pn}{p+n}\left(\frac{1}{1/v_{\mathrm{th}}\sigma_{\mathrm{o}}N_{\mathrm{t}}}\right) = \frac{pn}{(p+n)\tau_{\mathrm{nH}}}, \tag{5}$$

where $\tau_{\mathrm{nH}} = 1/v_{\mathrm{th}}\sigma_{\mathrm{o}}N_{\mathrm{t}}$ is the high-level injection lifetime for electron. There can be two levels of injection (external carrier entering into the device active regions). They are as follows:

1. *High-level injection*: Where the injected carrier density is comparable to the already existing doping density of that region;
2. *Low-level injection*: Where the injected carrier density is negligible compared to the already existing doping density of that region.

High-level injection assumption transforms (3) into a nonlinear second-order differential equation whose closed-form analytical solution cannot be obtained. But we can transform the mobility and diffusion coefficient values to take into account simultaneous presence of both electron and holes in high degree. We use *ambipolar mobility* (μ_{a}) *and diffusion coefficients* (D_{a}) instead of separate electron and hole mobility and diffusion coefficients. They are defined as follows:

$$\mu_{\mathrm{a}} = \frac{\mu_{\mathrm{n}}\mu_{\mathrm{p}}}{\mu_{\mathrm{n}} + \mu_{\mathrm{p}}}, \quad D_{\mathrm{a}} = \frac{\mu_{\mathrm{p}}D_{\mathrm{n}} + \mu_{\mathrm{n}}D_{\mathrm{p}}}{\mu_{\mathrm{n}} + \mu_{\mathrm{p}}}. \tag{6}$$

Therefore we can make the low-level injection assumption, i.e. the photogenerated carrier density is considerably less than the doping density in the P-type region. In that case, we can rewrite (5) as

$$\begin{aligned} R_{\mathrm{n,SRH}} &= \frac{pn}{p+n}\left(\frac{1}{1/v_{\mathrm{th}}\sigma_{\mathrm{o}}N_{\mathrm{t}}}\right) \\ &= \frac{n}{((p+n)/p)\tau_{\mathrm{nH}}} \approx \frac{n}{\tau_{\mathrm{nL}}}. \end{aligned} \tag{7}$$

Similarly, we obtain $R_{\mathrm{p,SRH}} \approx (p/\tau_{\mathrm{pL}})$. Here, τ_{nL} and τ_{pL} are low-level lifetimes for electrons and holes. The radiative recombination rate R_{rad} is same for electrons and holes and is given by [23]

$$R_{\mathrm{rad}} = C_{\mathrm{d}}(pn - n_{\mathrm{i}}^2), \tag{8}$$

where C_{d} is the radiative recombination coefficient. The photogeneration rate is same for electrons and holes and is given by [23]

$$G_{\mathrm{n}}(y) = G_{\mathrm{p}}(y) = \eta(1-R)\frac{P\lambda}{hc}\alpha\,\mathrm{e}^{-\alpha y} = G(y), \tag{9}$$

where η is the quantum efficiency, R is the surface reflectivity of the semiconductor, P is the optical power density, i.e. power incident on unit area, λ is the wavelength of the optical beam, α is the optical absorption coefficient, h and c denote Planck's constant and velocity of electromagnetic wave, respectively.

For steady-state analysis the time-dependent left-hand term in (3) is zero. Therefore, (3) transforms into a linear ordinary differential equation,

$$0 = D_a \frac{d^2 n}{dx^2} + \mu_a E \frac{dn}{dx} + G(y) - (R_{n,SRH} + R_{rad}). \tag{10}$$

Similar equation can be written for holes. Using (7), (8), and (9) in (10), we obtain the second-order ordinary differential equations governing the minority carrier densities, i.e. electron and hole concentrations in P-body and N-drift regions as

$$D_a \frac{d^2 n}{dx^2} + \mu_a E \frac{dn}{dx} - \left(\frac{1}{\tau_{nL}} + C_d N_{body}\right) n = -\left[G(y) + C_d n_i^2\right], \tag{11a}$$

$$D_a \frac{d^2 p}{dx^2} + \mu_a E \frac{dp}{dx} - \left(\frac{1}{\tau_{pL}} + C_d N_{drift}\right) p = -\left[G(y) + C_d n_i^2\right], \tag{11b}$$

where N_{body} and N_{drift} are majority carrier densities in P-body and N-drift regions, respectively. The solutions of (11) can be given as

$$n(x) = K_1 e^{m_1 x} + K_2 e^{m_2 x} + \frac{G(y) + C_d n_i^2}{\left((1/\tau_{nL}) + C_d N_{body}\right)},$$
$$p(x) = K_3 e^{m_3 x} + K_4 e^{m_4 x} + \frac{G(y) + C_d n_i^2}{\left((1/\tau_{pL}) + C_d N_{drift}\right)}. \tag{12}$$

In (12), K_1–K_4 are the constants to be determined from boundary conditions and so are dependent on specific geometry and doping definition of the device. The other constants are defined as follows:

$$m_1, m_2 = \frac{(-\mu_a E) \pm \sqrt{(\mu_a E)^2 + 4D_a\left((1/\tau_{nL}) + C_d N_{body}\right)}}{2D_a},$$
$$m_3, m_4 = \frac{(-\mu_a E) \pm \sqrt{(\mu_a E)^2 + 4D_a\left((1/\tau_{pL}) + C_d N_{drift}\right)}}{2D_a}. \tag{13}$$

For P-body and drift region, we calculate the averaged minority carrier densities as follows:

$$n_{body} = \frac{\int_0^{L_{body}} n(x)}{L_{body}} = \frac{m_1 K_1 e^{m_1 L_{body}} + m_2 K_2 e^{m_2 L_{body}} - (K_1 m_1 + K_2 m_2)}{L_{body}} + \frac{G(y) + C_d n_i^2}{\left((1/\tau_{nL}) + C_d N_{body}\right)}, \tag{14a}$$

$$p_{drift} = \frac{\int_0^{L_{drift}} p(x)}{L_{drift}} = \frac{m_3 K_3 e^{m_3 L_{drift}} + m_4 K_4 e^{m_4 L_{drift}} - (K_3 m_3 + K_4 m_4)}{L_{drift}} + \frac{G(y) + C_d n_i^2}{\left((1/\tau_{pL}) + C_d N_{drift}\right)}, \tag{14b}$$

where L_{body} and L_{drift} denote the length of P-body and N-drift regions, respectively. Two main components of the overall R_{on} are the P-body resistance (R_{body}) and N-drift resistance (R_{drift}) resulting in

$$R_{on} = R_{body} + R_{drift} = \frac{L_{body}}{\int_0^{d_1} q n_{body} \mu_a Z \, dy} + \frac{L_{drift}}{\int_0^{d_1} q p_{drift}(x) \mu_a Z \, dy}, \tag{15}$$

where q is the electronic charge, Z is the width of the device in Z-direction (perpendicular to the plane of the paper). Using the photogeneration function from (9), doing the integration, and substituting (14a) and (14b) in (15) we can write R_{on} in a compact form,

$$R_{on} = \frac{C_1 L_{body}}{C_1' + C_1'' P} + \frac{C_2 L_{drift}}{C_2' + C_2'' P}, \tag{16}$$

where

$$C_1 = \frac{1}{q Z \mu_a} = C_2, \tag{17a}$$

$$C_1' = \left[\frac{m_1 K_1 e^{m_1 L_{body}} + m_2 K_2 e^{m_4 L_{body}} - (K_1 m_1 + K_2 m_2)}{L_{body}} + \frac{C_d n_i^2}{\left((1/\tau_{nL}) + C_d N_{body}\right)}\right] d_1, \tag{17b}$$

$$C_2' = \left[\frac{m_3 K_3 e^{m_3 L_{drift}} + m_4 K_4 e^{m_4 L_{drift}} - (K_3 m_3 + K_4 m_4)}{L_{drift}} + \frac{C_d n_i^2}{\left((1/\tau_{pL}) + C_d N_{drift}\right)}\right] d_1, \tag{17c}$$

$$C_1'' = \frac{\eta(1-R)\lambda\left(1 - e^{-\alpha d_1}\right)}{hc\left(\frac{1}{\tau_{nL}} + C_d N_{body}\right)},$$
$$C_2'' = \frac{\eta(1-R)\lambda\left(1 - e^{-\alpha d_1}\right)}{hc\left(\frac{1}{\tau_{pL}} + C_d N_{drift}\right)} \tag{17d}$$

From (2), the transcendental equation relating L_{drift} and V_{Br} is,

$$2.994 \times 10^5 \exp\left(-\left(6.648 \times 10^5 L_{drift}/V_{Br}\right)^{1.6}\right) + 2.215 \times 10^5 \exp\left(-\left(6.57 \times 10^5 L_{drift}/V_{Br}\right)^{1.75}\right) = \frac{1}{L_{drift}}. \tag{18}$$

Therefore, (16) and (18) illustrate that variation of R_{on} with V_{Br} can be modulated by P because R_{on} is related to L_{drift} by a parameter containing P.

3.2. Switching times modulated by optical power density

Transient modeling of the OTPT dynamics requires time-dependent carrier density calculation as a function of optical power density. The P-body region is critical in determining the transient dynamics because it strongly influences the recombination rate. At first, we consider high-level injection case. The diffusion terms involving $\partial n/\partial x$ and its derivative in (3) can be considered negligible (because of uniform carrier density in the P-body region) and we can write the time-varying equation in the P-body region as

$$\frac{\mathrm{d}n}{\mathrm{d}t} = G_{\mathrm{opt}} - \frac{N_{\mathrm{body}}n}{(N_{\mathrm{body}}+n)\tau_{\mathrm{nH}}} - C_{\mathrm{d}}(N_{\mathrm{body}}n - n_{\mathrm{i}}^2). \tag{19}$$

Ion implantation was done to realize the P-body region in the fabricated prototype and in that case the average acceptor density can be given as

$$N_{\mathrm{body}} = \frac{\int_0^{R_{\mathrm{body}}} (Q_{\mathrm{body}}/\Delta R_{\mathrm{body}}\sqrt{2\pi})\exp\left[\left(-(y-R_{\mathrm{body}})^2\right)/2\Delta R_{\mathrm{body}}^2\right]}{R_{\mathrm{body}}}, \tag{20}$$

where Q_{body} is implantation dose for P-body, R_{body} is implant range for P-body (for a particular species of ion), and ΔR_{body} is lateral struggle for P-body implantation. The spatially averaged photogeneration rate G_{opt} can be given as

$$G_{\mathrm{opt}} = \frac{\int_0^{d_1} G(y)\,\mathrm{d}y}{\int_0^{d_1}\mathrm{d}y} = \eta(1-R)\frac{P\lambda}{hc}\left(\frac{1-\mathrm{e}^{-\alpha d_1}}{d_1}\right), \tag{21}$$

where photogeneration rate (which varies with the depth) is averaged over the thickness (d_1) of the optical absorption layer, i.e. N-GaAs layer. Separating the variables in (19), we obtain,

$$\int \frac{\tau_{\mathrm{nH}}(N_{\mathrm{body}}+n)\,\mathrm{d}n}{-C_{\mathrm{d}}\tau_{\mathrm{n}}N_{\mathrm{body}}n^2 + (G_{\mathrm{opt}}\tau_{\mathrm{nH}} - N_{\mathrm{body}} - C_{\mathrm{d}}N_{\mathrm{body}}^2\tau_{\mathrm{nH}})n + G_{\mathrm{opt}}N_{\mathrm{body}}\tau_{\mathrm{nH}}} = \int \mathrm{d}t, \tag{22}$$

We assume the initial condition $n(t=0)=0$ (because initially the electron concentration in the P-body region is negligibly small, e.g. $n_{\mathrm{i}}^2/p \approx (2.1\times10^6)^2/10^{17} \approx 4.41\times10^{-5}$). The integration constant k is obtained as

$$k = \tau_{\mathrm{nH}}\left[\frac{1}{2a}\ln(c) + \left(p - \frac{b}{2a}\right)\left(\frac{1}{\sqrt{b^2-4ac}}\right) \times \ln\left(\frac{b-\sqrt{b^2-4ac}}{b+\sqrt{b^2-4ac}}\right)\right] \tag{24}$$

where the constants a, b, c are given by,

$$\begin{aligned} a &= -C_{\mathrm{d}}\tau_{\mathrm{nH}}N_{\mathrm{body}}, \\ b &= G_{\mathrm{opt}}\tau_{\mathrm{nH}} - N_{\mathrm{body}} - C_{\mathrm{d}}\tau_{\mathrm{nH}}N_{\mathrm{body}}^2, \\ c &= G_{\mathrm{opt}}N_{\mathrm{body}}\tau_{\mathrm{nH}}. \end{aligned} \tag{25}$$

Therefore, using (24) in (23) and the definitions of (25), the final transcendental time-domain equation governing electron density can be written as

$$\tau_{\mathrm{nH}}\left[\frac{1}{2a}\ln\left(\frac{an^2+bn+c}{c}\right) + \left(p-\frac{b}{2a}\right)\left(\frac{1}{\sqrt{b^2-4ac}}\right) \times \ln\left(\frac{\left(2an+b-\sqrt{b^2-4ac}\right)\left(b+\sqrt{b^2-4ac}\right)}{\left(2an+b+\sqrt{b^2-4ac}\right)\left(b-\sqrt{b^2-4ac}\right)}\right)\right] = t. \tag{26}$$

We calculate rise time from the switching simulations done using OTPT device model in a mixed circuit-device simulator. A resistive load circuit is used as shown in Fig. 5a. Rise time is defined as the time taken to reach the electron density from 0% to 95% of its final value (as shown in Fig. 5b), which we denote as n_{F}. Final electron density value is determined by the circuit and we can approximately calculate that from the resistance of the OTPT. For example, we obtained $0.2\,\Omega$ resistance for a Z-direction length of $5\times10^5\,\mu\mathrm{m}$. The GaAs layer depth is $1\,\mu\mathrm{m}$. Thus, the cross-sectional area (A_{c}) through which carriers are traveling is, $(5\times10^5\times1)\,\mu\mathrm{m}^2$ or equivalently $(50\times10^{-4}\,\mathrm{cm}^2)$. The length of the P-body region is $5\,\mu\mathrm{m}$.

$$\begin{aligned} &-\frac{1}{2C_{\mathrm{d}}\tau_{\mathrm{nH}}N_{\mathrm{body}}}\ln\left[-C_{\mathrm{d}}\tau_{\mathrm{nH}}N_{\mathrm{body}}n^2 + (G_{\mathrm{opt}}\tau_{\mathrm{nH}} - N_{\mathrm{body}} - C_{\mathrm{d}}\tau_{\mathrm{nH}}N_{\mathrm{body}}^2)n + G_{\mathrm{opt}}N_{\mathrm{body}}\tau_{\mathrm{nH}}\right] \\ &+\left(N_{\mathrm{body}} + \frac{G_{\mathrm{opt}}\tau_{\mathrm{nH}} - N_{\mathrm{body}} - C_{\mathrm{d}}\tau_{\mathrm{nH}}N_{\mathrm{body}}^2}{2C_{\mathrm{d}}\tau_{\mathrm{nH}}N_{\mathrm{body}}}\right) \\ &\left[\frac{\ln\left(\dfrac{2C_{\mathrm{d}}\tau_{\mathrm{nH}}N_{\mathrm{body}}n + G_{\mathrm{opt}}\tau_{\mathrm{nH}} - N_{\mathrm{body}} - C_{\mathrm{d}}\tau_{\mathrm{nH}}N_{\mathrm{body}}^2 - \sqrt{\left(G_{\mathrm{opt}}\tau_{\mathrm{nH}} - N_{\mathrm{body}} - C_{\mathrm{d}}\tau_{\mathrm{nH}}N_{\mathrm{body}}^2\right)^2 + 4G_{\mathrm{opt}}C_{\mathrm{d}}\tau_{\mathrm{nH}}^2N_{\mathrm{body}}^2}}{2C_{\mathrm{d}}\tau_{\mathrm{nH}}N_{\mathrm{body}}n + G_{\mathrm{opt}}\tau_{\mathrm{nH}} - N_{\mathrm{body}} - C_{\mathrm{d}}\tau_{\mathrm{nH}}N_{\mathrm{body}}^2 + \sqrt{\left(G_{\mathrm{opt}}\tau_{\mathrm{nH}} - N_{\mathrm{body}} - C_{\mathrm{d}}\tau_{\mathrm{nH}}N_{\mathrm{body}}^2\right)^2 + 4G_{\mathrm{opt}}C_{\mathrm{d}}\tau_{\mathrm{nH}}^2N_{\mathrm{body}}^2}}\right)}{\sqrt{\left(G_{\mathrm{opt}}\tau_{\mathrm{nH}} - N_{\mathrm{body}} - C_{\mathrm{d}}\tau_{\mathrm{nH}}N_{\mathrm{body}}^2\right)^2 + 4G_{\mathrm{opt}}C_{\mathrm{d}}\tau_{\mathrm{nH}}^2N_{\mathrm{body}}^2}}\right] = \frac{t+k}{\tau_{\mathrm{nH}}}. \end{aligned} \tag{23}$$

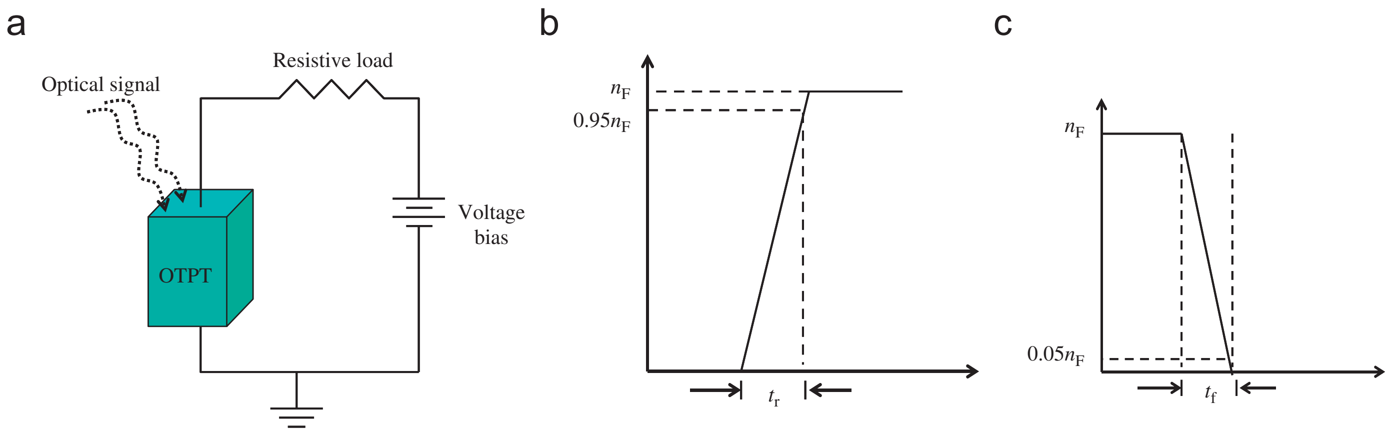

Fig. 5. (a) Switching simulation circuit for OTPT and definitions of (b) rise time and (c) fall time.

The electron density can be calculated as

$$n_F = \frac{L_{body}}{R_{on}A_c q\mu_a} = \frac{5\times10^{-4}\,\text{cm}}{0.2\,\Omega\times(50\times10^{-4})\,\text{cm}^2\times1.602\times10^{-19}\,\text{C}\times2000\,\text{cm}^2/\text{V}} = 1.56\times10^{15}\,\text{cm}^{-3}.$$

The equation relating t_r and P can be given as

$$t_r = \tau_{nH}\left[\frac{1}{2a}\ln\left(\frac{a(0.95n_F)^2+b(0.95n_F)+c}{c}\right) + \left(p-\frac{b}{2a}\right)\left(\frac{1}{\sqrt{b^2-4ac}}\right) \times\ln\left(\frac{\left(2a(0.95n_F)+b-\sqrt{b^2-4ac}\right)\left(b+\sqrt{b^2-4ac}\right)}{\left(2a(0.95n_F)+b+\sqrt{b^2-4ac}\right)\left(b-\sqrt{b^2-4ac}\right)}\right)\right], \tag{27}$$

$$t_r = \tau_{nH}\left[\ln\left(\frac{M_1P+M_2}{M_3P}\right)^{M_4} + \frac{(M_5P+M_6)}{\sqrt{M_7P^2+M_8}} \times\ln\left(\frac{M_9P+M_{10}-\sqrt{M_7P^2+M_8}}{M_9P+M_{10}+\sqrt{M_7P^2+M_8}}\right)\right], \tag{28}$$

where $M_j, j=1,2,\ldots,10$ are different constants that can be evaluated using (21), (25), and (27). We define fall-time as the time taken to reach the electron density to 5% of its final value (as shown in Fig. 5c) after the light is shut off. Therefore, for the OTPT turn-off, we can re-write (19) as

$$\frac{dn}{dt} = -\frac{N_{body}n}{(N_{body}+n)\tau_{nH}} - C_d(N_{body}n - n_i^2). \tag{29}$$

Solving (29) in a similar manner and using the initial condition $n(t=0)=n_F$, we obtain the fall-time as

$$t_f = \tau_{nH}\left[S_1 + S_2\ln\left(\frac{An_F+B}{A(0.05n_F)+B}\right)\right], \tag{30}$$

where A, B, S_1 and S_2 are constants and are given by

$$A = C_dN_{body}\tau_{nH},$$
$$B = C_dN_{body}^2\tau_{nH} + N_{body},$$
$$S_1 = \frac{N_{body}\ln(20)}{N_{body}+C_dN_{body}^2\tau_{nH}},$$
$$S_2 = \frac{1}{C_dN_{body}\tau_{nH}} - \frac{N_{body}}{N_{body}+C_dN_{body}^2\tau_{nH}}. \tag{31}$$

Apparently P does not influence t_f, but because the final electron density in conduction state is influenced by the optical power density (as apparent from the R_{on} variation with P following the analysis in the previous subsection), it does have an effect on the fall-time.

The closed-form solution of (19) can be considerably simplified in the low-level injection case where the equation changes to,

$$\frac{dn}{dt} = G_{opt} - \frac{n}{\tau_{nL}} - C_d(N_{body}n - n_i^2). \tag{32}$$

Neglecting n_i^2 compared to pn (as done before) and taking the same initial condition we can write the general solution of (32) as,

$$n(t) = \frac{G_{opt}}{((1/\tau_{nL})+C_dN_{body})}\left[1 - e^{-((1/\tau_{nL})+C_dN_{body})t}\right]. \tag{33}$$

Rise time can be calculated as,

$$t_r = \frac{\tau_{nL}}{1+\tau_{nL}C_dN_{body}} \times\ln\left(\frac{G_{opt}}{G_{opt}-((1/\tau_{nL})+C_dN_{body})(0.95n_F)}\right). \tag{34}$$

We can write (34) in terms of P as

$$t_r = F_1\ln\left(\frac{F_2P}{F_2P-F_3}\right), \tag{35}$$

where F_1, F_2, and F_3 are constants and are given by

$$F_1 = \frac{\tau_{\mathrm{nL}}}{1 + \tau_{\mathrm{nL}} C_{\mathrm{d}} N_{\mathrm{body}}},$$
$$F_2 = \eta(1 - R)\frac{\lambda}{hc}\left(\frac{1 - \mathrm{e}^{-\alpha d_1}}{d_1}\right),$$
$$F_3 = \frac{(1 + \tau_{\mathrm{nL}} C_{\mathrm{d}} N_{\mathrm{body}})(0.95 n_{\mathrm{F}})}{\tau_{\mathrm{nL}}}. \quad (36)$$

An interesting observation can be made from (28) and (35). The value of t_{r} in the limit of very large P, is zero as predicted by (35), because $\lim_{P\to\infty}(t_{\mathrm{r}}) = F_1 \ln\big((F_2 P / F_2 P)\big) = 0$. On the other hand, (28) predicts a small but finite value as

$$\lim_{P\to\infty}(t_{\mathrm{r}}) = \tau_{\mathrm{nH}}\left[\ln\left(\frac{M_1}{M_3}\right)^{M_4} + \left(\frac{M_5}{M_7}\right)\ln\left(\frac{M_9 - M_7}{M_9 + M_7}\right)\right]. \quad (37)$$

This is more realistic because physically when the generation is very large, so is the recombination rate and there must be a finite time for the carrier density to reach the steady-state value.

3.3. *On-state resistance and switching time modulated by optical wavelength*

Analyses in the previous two sections demonstrate that R_{on} and switching times of OTPT depends on the photogeneration rate, which, in turn, depends on the wavelength (λ), absorption coefficient (α), and surface reflectivity (R) according to (9). Furthermore, both α and R is nonlinear function of λ. Functional dependence of α on λ can be expressed using Tharmalingam model [24]:

$$\alpha(\lambda, E) = \frac{q^2 C_0^2 (2m_{\mathrm{r}}/\hbar)^{3/2}}{\pi\hbar c^2 n m_{\mathrm{e}}^2}\left(\frac{q^2E^2}{2m_{\mathrm{r}}\hbar}\right)^{1/6} \times \left[\left|\frac{\mathrm{dAi}(\beta)}{\mathrm{d}\beta}\right|^2 - \beta\left|\mathrm{Ai}(\beta)\right|^2\right], \quad (38)$$

where

$$\beta = \left[E_{\mathrm{g}} - (hc/\lambda)\right] \Big/ \hbar\left(\frac{q^2E^2}{2m_{\mathrm{r}}\hbar}\right)^{1/3}$$

and $\mathrm{Ai}(\beta)$ is the Airy function defined by $\mathrm{Ai}(\beta) = \frac{1}{\sqrt{\pi}}\int_0^\infty \cos\left(\frac{1}{3}u^3 + u\beta\right)\mathrm{d}u$. In (38), E_{g} is the bandgap, m_{r} is reduced mass of electron–hole pair, m_{e} is electron mass, C_0 is the momentum element for electron transfer between two allowed states. Surface reflectivity R is given by [25],

$$R(\lambda) = \frac{\varepsilon_{\mathrm{i}}(\lambda)^2 + \left(\varepsilon_{\mathrm{r}}(\lambda) - 1/\cos\theta\right)^2}{\varepsilon_{\mathrm{i}}(\lambda)^2 + \left(\varepsilon_{\mathrm{r}}(\lambda) + 1/\cos\theta\right)^2}, \quad (39)$$

where θ is the angle of incidence, and $\varepsilon_{\mathrm{r}}(\lambda)$ and $\varepsilon_{\mathrm{i}}(\lambda)$ are the real and imaginary parts of the complex dielectric function, respectively. R changes with incident λ (due to the change in the dielectric function value [26]) and the variation for GaAs is plotted in Fig. 6a, using the data from [27].

We can explicitly write the governing equations for the wavelength modulated properties as

$$R_{\mathrm{on}} = \frac{C_1}{C_1' + D_1(1 - R(\lambda))\lambda(1 - \mathrm{e}^{-\alpha(\lambda)d_1})}, \quad (40)$$

$$t_{\mathrm{r}} = \tau_{\mathrm{nH}}\left[\ln\left(\frac{M_1'\big((1-R(\lambda))\lambda\big(1-\mathrm{e}^{-\alpha(\lambda)d_1}\big)\big)+M_2}{M_3'\big((1-R(\lambda))\lambda\big(1-\mathrm{e}^{-\alpha(\lambda)d_1}\big)\big)}\right)^{M_4} + \frac{\big(M_5'\big((1-R(\lambda))\lambda\big(1-\mathrm{e}^{-\alpha(\lambda)d_1}\big)\big)+M_6\big)}{\sqrt{M_7'\big((1-R(\lambda))\lambda\big(1-\mathrm{e}^{-\alpha(\lambda)d_1}\big)\big)^2+M_8}} \ln\left(\frac{M_9'\big((1-R(\lambda))\lambda\big(1-\mathrm{e}^{-\alpha(\lambda)d_1}\big)\big)+M_{10}-\sqrt{M_7'\big((1-R(\lambda))\lambda\big(1-\mathrm{e}^{-\alpha(\lambda)d_1}\big)\big)^2+M_8}}{M_9'\big((1-R(\lambda))\lambda\big(1-\mathrm{e}^{-\alpha(\lambda)d_1}\big)\big)+M_{10}+\sqrt{M_7'\big((1-R(\lambda))\lambda\big(1-\mathrm{e}^{-\alpha(\lambda)d_1}\big)\big)^2+M_8}}\right)\right] \quad (41)$$

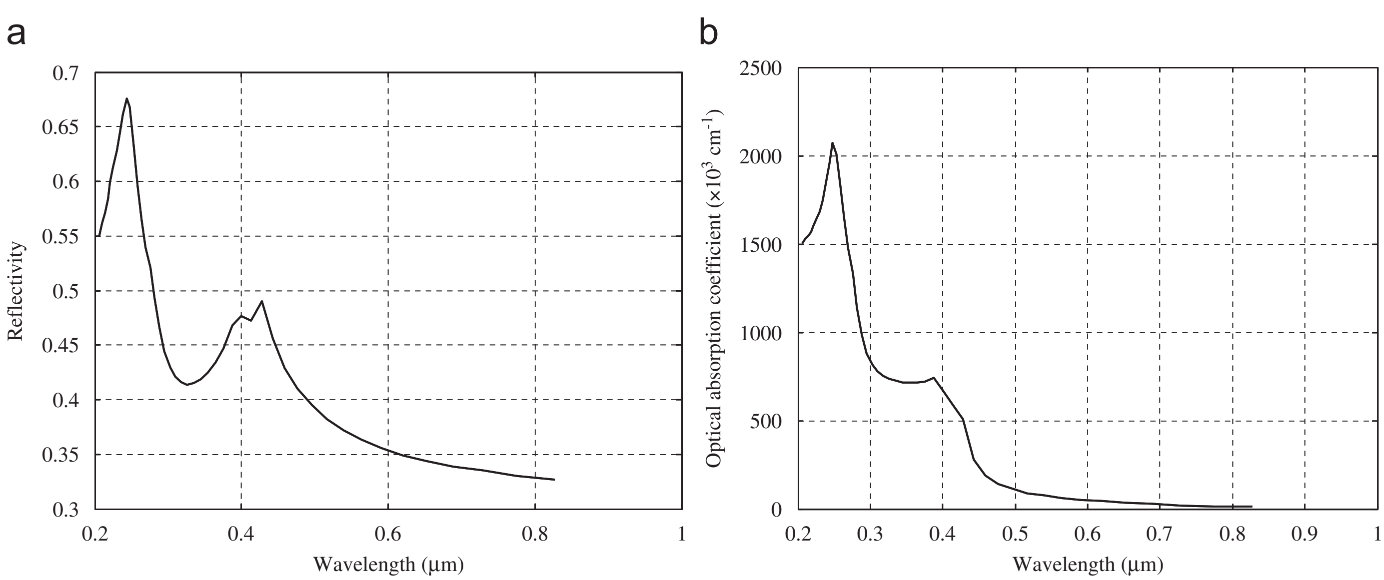

Fig. 6. GaAs (a) surface reflectivity and (b) optical absorption coefficient, as the function of optical wavelength.

or for low-level injection case

$$t_{\mathrm{r}} = F_1 \ln\left(\frac{F_2'(1-R(\lambda))\lambda\left(1-\mathrm{e}^{-\alpha(\lambda)d_1}\right)}{F_2'(1-R(\lambda))\lambda(1-\mathrm{e}^{-\alpha(\lambda)d_1}) - F_3}\right), \tag{42}$$

where $F_2' = \eta(P/hcd_1)$. M_1', M_3', M_5', M_7', and M_9' are related to M_1, M_3, M_5, M_7, and M_9 as

$$M_j' = \frac{M_j P}{(1-R(\lambda))\lambda(1-\mathrm{e}^{-\alpha(\lambda)d_1})},$$

where $j \in \{1,3,5,7,9\}$.

3.4. Rise time modulated by optical signal rise time

To vary the rise time of a conventional power MOSFET, gate resistance needs to be changed physically to alter the rate of charging the gate capacitance. For OTPT, simply by varying the triggering laser rise time, the main device rise time can be changed dynamically. This is because rise time of OTPT depends on how fast the photogenerated charges build up to create the channel. This rate is directly proportional to the rate of rise of time-dependent optical power density. We can write the governing equation by replacing the constant photogeneration term in (19) by a linear ramp-type time-dependent term (only for the time period of rising edge),

$$\frac{\mathrm{d}n}{\mathrm{d}t} = \frac{G_0 t}{t_0} - \frac{N_{\mathrm{body}} n}{(N_{\mathrm{body}}+n)\tau_{\mathrm{nH}}} - C_{\mathrm{d}}\left(N_{\mathrm{body}} n - n_{\mathrm{i}}^2\right), \tag{43}$$

where G_0 is the final value of the ramped-up photogeneration rate and t_0 is the time taken by the optical signal to reach this value. Separation of variables is not possible in this case and therefore (43) leads to a nonlinear Abel's equation,

$$\begin{aligned} &n\frac{\mathrm{d}n}{\mathrm{d}t} + N_{\mathrm{body}}\frac{\mathrm{d}n}{\mathrm{d}t} \\ &= N_{\mathrm{body}}\frac{G_0 t}{t_0} + n\left(\frac{G_0 t}{t_0} - \frac{N_{\mathrm{body}}}{\tau_{\mathrm{n}}} - C_{\mathrm{d}} N_{\mathrm{body}}^2\right) \\ &\quad - C_{\mathrm{d}} N_{\mathrm{body}} n^2. \end{aligned} \tag{44}$$

Because of the lack of analytical closed-form solution for (44), we study the rise time variation by numerical simulation. But, for low-level injection, (43) can be re-written as

$$\frac{\mathrm{d}n}{\mathrm{d}t} = \frac{G_0 t}{t_0} - \frac{n}{\tau_{\mathrm{nL}}} - C_{\mathrm{d}}(N_{\mathrm{body}} n - n_{\mathrm{i}}^2). \tag{45}$$

Neglecting the n_{i}^2 for the identical reason, as explained before, we obtain,

$$\frac{\mathrm{d}n}{\mathrm{d}t} = \frac{G_0 t}{t_0} - n\left(\frac{1}{\tau_{\mathrm{nL}}} + C_{\mathrm{d}} N_{\mathrm{body}}\right). \tag{46}$$

The general solution of (46) with the initial condition of $n(t=0)=0$ is given by,

$$n(t) = \frac{G_0}{t_0\left((1/\tau_{\mathrm{nL}}) + C_{\mathrm{d}} N_{\mathrm{body}}\right)^2} \times \left[\left((1/\tau_{\mathrm{nL}}) + C_{\mathrm{d}} N_{\mathrm{body}}\right)t + \mathrm{e}^{-\left((1/\tau_{\mathrm{nL}})+C_{\mathrm{d}}N_{\mathrm{body}}\right)t} - 1\right]. \tag{47}$$

To obtain the rise time, we first calculate the electron density value as same as 95% of the final electron density value at $t = t_0$, and equate that to the electron density value at $t = t_{\mathrm{r}}$

$$\frac{G_0}{t_0\left((1/\tau_{\mathrm{nL}}) + C_{\mathrm{d}} N_{\mathrm{body}}\right)^2} \times \left[\left(\frac{1}{\tau_{\mathrm{nL}}} + C_{\mathrm{d}} N_{\mathrm{body}}\right)t_{\mathrm{r}} + \mathrm{e}^{-\left((1/\tau_{\mathrm{nL}})+C_{\mathrm{d}}N_{\mathrm{body}}\right)t_{\mathrm{r}}} - 1\right] = 0.95 n_{\mathrm{F}}. \tag{48}$$

The solution of the transcendental equation (48) can be given in terms of *Lambert's W*-function [28] as

$$t_{\mathrm{r}} = \frac{1}{\left((1/\tau_{\mathrm{nL}}) + C_{\mathrm{d}} N_{\mathrm{body}}\right)}\left[1 + \frac{t_0\left((1/\tau_{\mathrm{nL}}) + C_{\mathrm{d}} N_{\mathrm{body}}\right)^2}{G_0} + W\left(-\exp\left(-1 - \frac{t_0\left((1/\tau_{\mathrm{nL}}) + C_{\mathrm{d}} N_{\mathrm{body}}\right)(0.95 n_{\mathrm{F}})}{G_0}\right)\right)\right], \tag{49}$$

where the W-function is given by,

$$W(x) = \sum_{n=1}^{\infty} \frac{(-1)^{n-1} n^{n-2}}{(n-1)!} x^{n-2}. \tag{50}$$

Eq. (49) shows the influence of material property such as τ_{nL} and C_{d}, design parameter such as N_{body}, and triggering parameter such as t_0, on the rise time of the main power device. It also predicts that for a given t_0, t_{r} can be reduced by increasing G_0.

4. Results and discussion

ATLAS framework is used to conduct two-dimensional ()finite-element switching simulations of OTPT. Table 1 details the design and fabrication parameters for the device model constructed in ATHENA process simulator. The nonlinear variation of reflectivity R and optical absorption coefficient α with wavelength λ is modeled by defining the corresponding values for a range of wavelengths in a separate data file which is read while simulation.

Analytical calculations were done and numerical simulations were carried out to show (in Fig. 7a) the variation of R_{on} with P for a 600 V, 10 A OTPT. Further, it is shown in Fig. 7b how the R_{on} vs. V_{Br} curve can be modulated with different values of P. Drift length of the OTPT was varied over a range of 15–80 μm to obtain varying breakdown voltages and each model is subjected to switching simulation to estimate R_{on}. This modulation is unique to direct optically controlled devices like OTPT and has no analogue in electrically controlled power devices.

Switching simulations were carried out incorporating the device model into MixedMode circuit simulator of ATLAS to estimate the switching time variations with P and the results are plotted in Figs. 8a and b. At lower P, the variation slightly deviates from the theoretically predicted logarithmic curve because the final current (therefore the

Table 1
Process simulation parameters for the OTPT model in ATHENA and ATLAS

Parameter	Value	Parameter	Value	Parameter	Value
P-AlGaAs thickness	300 nm	P-body length	5 μm	Drain length	20 μm
N-GaAs thickness	1 μm	P-body implant dose	$1\times10^{13}\,cm^{-2}$	Drain implant dose	$5\times10^{14}\,cm^{-2}$
N-AlGaAs thickness	100 nm	P-body implant energy	150 keV	Drain implant energy	100 keV
P-AlGaAs doping	$10^{15}\,cm^{-3}$	Source length	20 μm	Activation time	5 min
N-GaAs doping	$2\times10^{14}\,cm^{-3}$	Source implant dose	$5\times10^{14}\,cm^{-2}$	Activation temp.	850 °C
N-AlGaAs doping	$10^{15}\,cm^{-3}$	Source implant energy	100 keV	AR coating thickness	100 nm
Drift length	35 μm	N-type implant ion	Si	P-type implant ion	Be

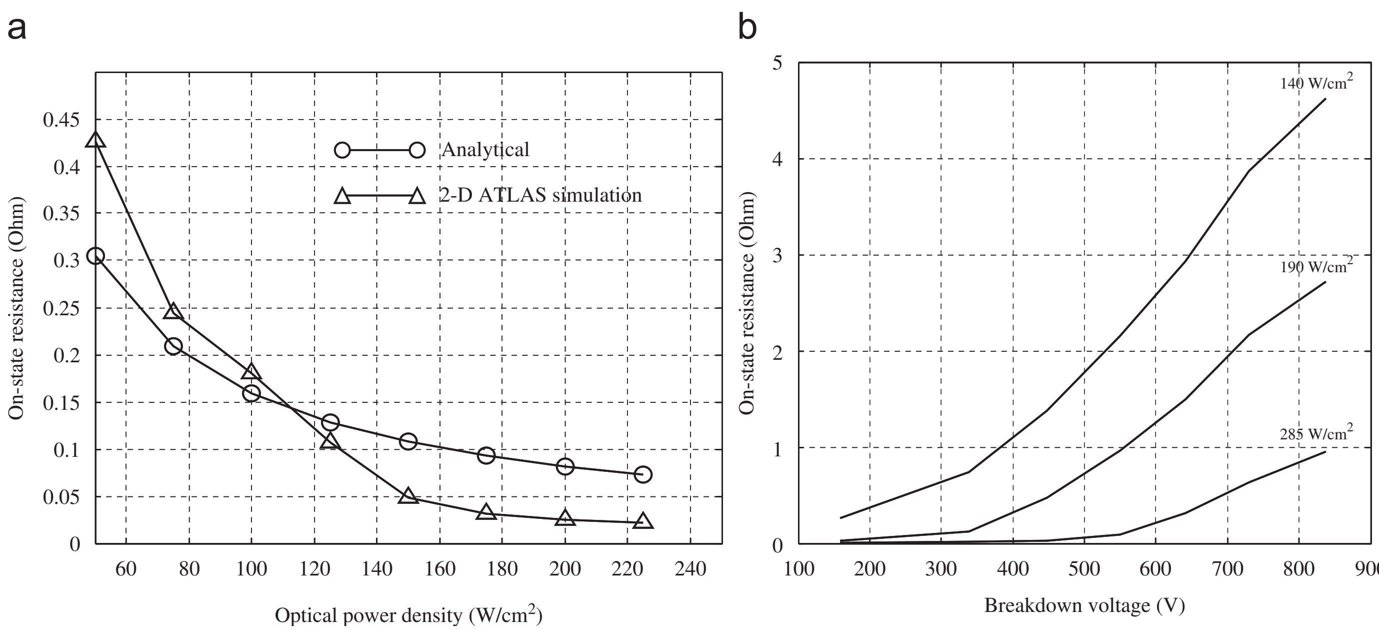

Fig. 7. (a) On-state resistance vs. optical power density and (b) on-state resistance vs. breakdown voltage for different optical power densities.

final carrier density) becomes less (as shown in Fig. 9) and the assumption of a fixed n_F does not hold true. Percentage variation of t_f with P is much less than the corresponding variation of t_r, as predicted by the theoretical analysis. For the same P variation of 50–225 W/cm^2, t_r decreases from 8.7 to 3.05 ns (a change of 65% over the initial value) whereas t_f increases from 26.4 to 29.6 ns (a change of 12% over the initial value). Fig. 9 shows the turn-off dynamics of OTPT for different P indicating that for higher P, the delay between the optical signal turn-off and actual device turn-off increases due to enhanced recombination phase of higher density of photogenerated carriers.

We carried out number of switching simulations of the OTPT varying the wavelength of the optical triggering signal over the range of 700–850 nm and extracted corresponding R_{on} and switching time data. Influence of λ on the R_{on} and the t_r and t_f of OTPT can be seen from Figs. 10a and b. At lower wavelengths, there are two reasons for high R_{on}. Firstly, for the same optical power density, number of photons is less and thus photogenerated carrier density becomes smaller leading to higher R_{on}. Secondly, $R(\lambda)$ also increases in that range, reducing the effective optical absorption. For λ greater than the absorption edge (around 820 nm for GaAs) α decreases rapidly and so does the photogeneration rate. This again leads to higher R_{on} due to less effective carrier density. An inversion point in the R_{on} curve is observed around 820–840 nm wavelength region.

Fig. 11a illustrates the variation of OTPT rise time with optical trigger rise time variation in a time-domain plot. In Fig. 11b parametric plot is shown for the corresponding quantities for three different optical power levels. For the same t_0, shorter t_r can be obtained by providing higher optical power, as expected from the theoretical analysis.

5. Summary and conclusion

Optical modulation techniques, that can be applied to dynamically alter power device performance, have been discussed with respect to GaAs/AlGaAs based OTPT. One-dimensional drift-diffusion equation is solved along with the photogeneration term to estimate the effect of optical

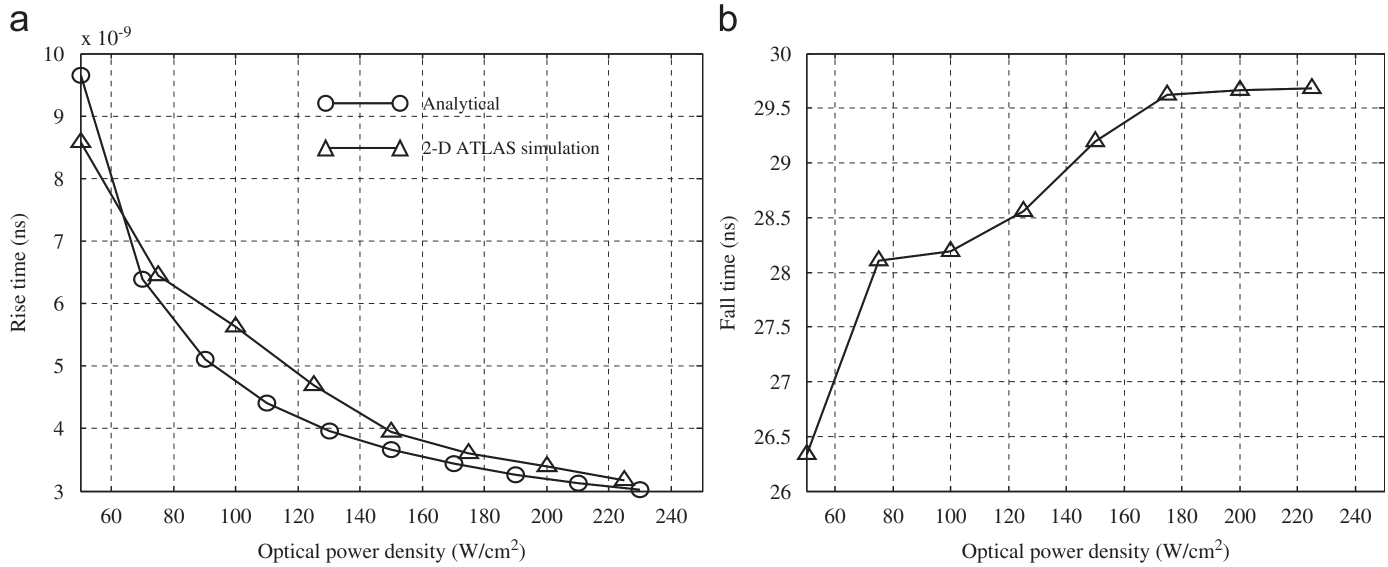

Fig. 8. Variation of OTPT (a) rise time and (b) fall time with optical power density.

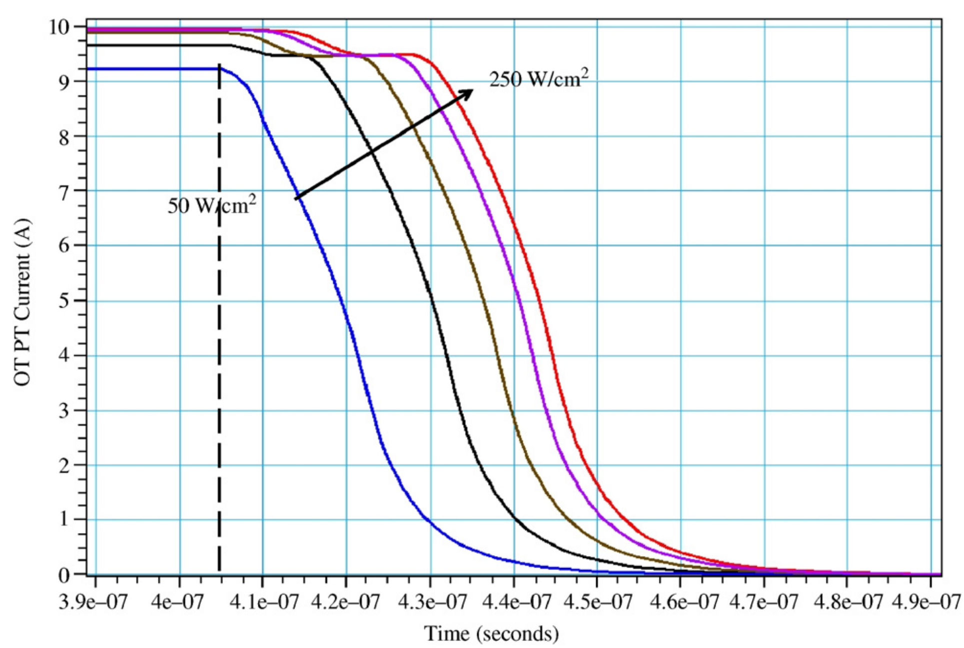

Fig. 9. OTPT turn-off dynamics for different optical power densities varying from 50 to 250 W/cm^2. The optical signal turns off at the time instant of 4.05×10^{-7} s (indicated by the dotted vertical line). Higher optical power density results in higher carrier density during conduction state which causes a higher delay before the current starts decaying by recombination process after the optical signal turns off.

parameters on OTPT performance parameters such as on-state resistance (R_{on}) and rise time (t_r) and fall time (t_f). Due to direct bandgap nature of GaAs, both SRH and radiative recombination mechanisms have been included in the analysis. A summary of the key findings is presented in Table 2.

Optical triggering power density P is found to modulate the R_{on} through a hyperbolic functional dependence and a saturated behavior is observed in the variation of R_{on} above a certain value of P. More importantly, the trade-off curve between the breakdown voltage V_{Br} and R_{on} is also shown to be modulated by P.

Solution of non-steady-state continuity equation with high-level injection condition yields a transcendental equation governing the time-varying electron density and predicts a logarithmic variation of rise time t_r with P. Numerical simulations confirm this prediction. Theoretical analysis also predicts a small but finite value of rise time for arbitrarily large P and asserts that above a certain threshold increasing P will not decrease t_r significantly.

Optical wavelength λ alters R_{on} and t_r and t_f in nonlinear fashion. Apart from the straightforward linear variation in the effective photon density (for a fixed optical power), this nonlinear variation can be attributed to change in optical

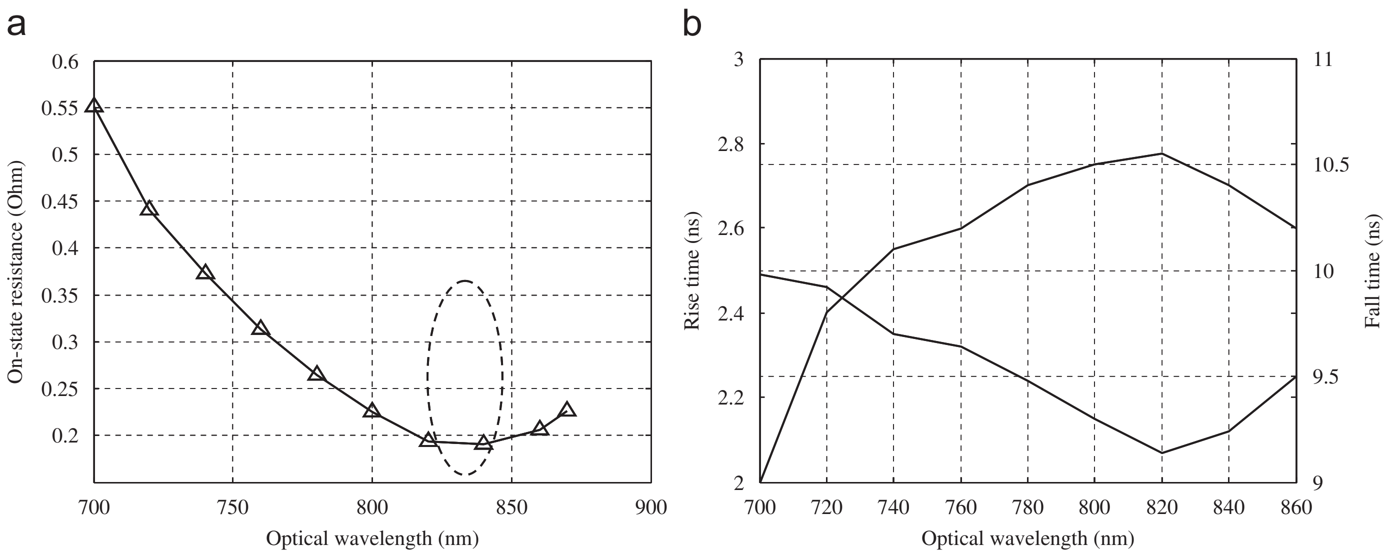

Fig. 10. Modulation of OTPT (a) on-state resistance and (b) switching times by optical wavelength variation.

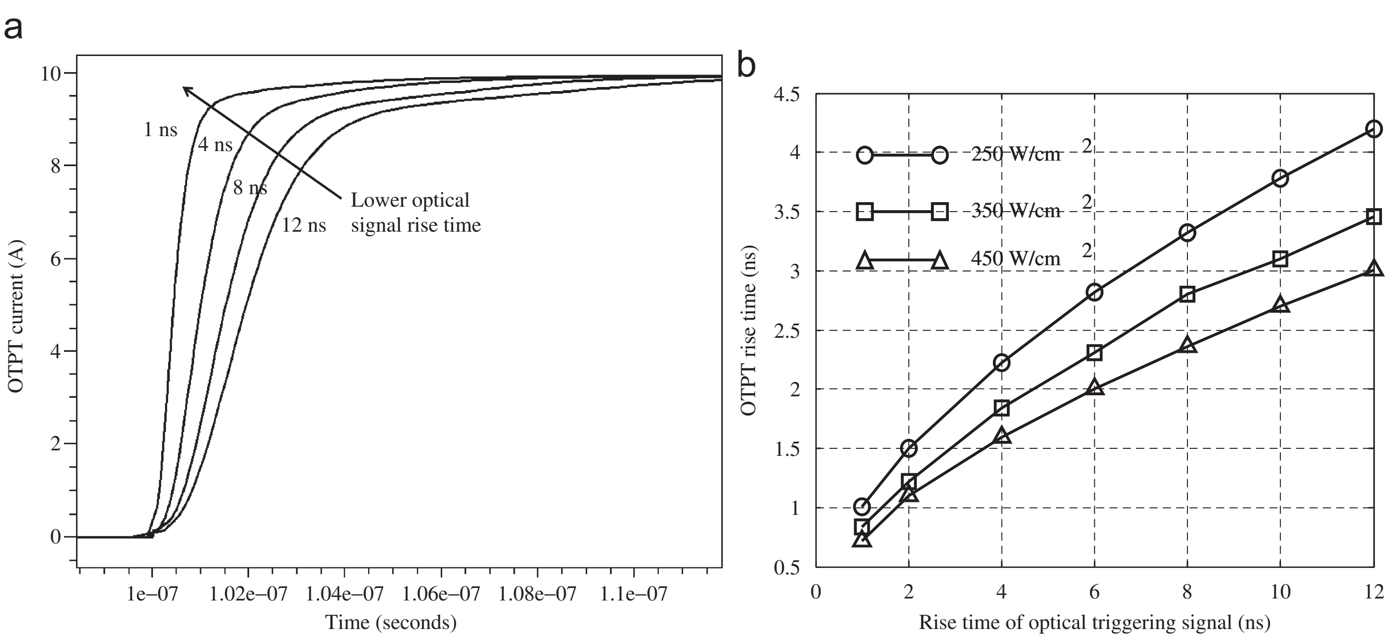

Fig. 11. (a) OTPT rise time modulation by varying optical trigger rise time and (b) rise time variation for different optical power densities.

Table 2
Summary of optical modulation effects on OTPT and functional dependence

Parameters	Power density	Wavelength	Rise time
On-state resistance	Strongly affects, Eq. (16), functional dependence hyperbolic	Strongly affects, Eq. (40), nonlinear	Does not affect
Rise time	Strongly affects, Eqs. (28) or (35), functional dependence logarithmic	Slightly affects, Eqs. (41) or (42), nonlinear	Strongly affects, Eq. (49), functional dependence Lambert *W*-function
Fall time	Indirectly affects, Eq. (30)	Indirectly affects, nonlinear	NA

absorption coefficient α and surface reflectivity R with λ. Simulations show a minimum of R_{on} at around 820 nm for OTPT.

OTPT rise time exhibits strong dependence on the rate of rise of the optical signal because of the direct photogeneration induced switching and absence of any capacitive structure such as MOSFET gate. It was shown that they can be approximately related by Lambert's *W*-function with exponential coefficient. Also, for the same optical signal rise time, shorter t_r can be achieved by higher optical power.

Apart from predicting the effect of optical parameter variation, analytical modeling helps to identify critical device design parameters that influence the switching and steady-state performance strongly. Most prominent examples are P-body doping density or N-GaAs layer thickness appearing in the governing equations for R_{on} or t_r This knowledge helps to choose a particular fabrication methodology (for example a particular ion species for implantation or a specific epitaxial growth technique) for achieving suitable device dimension and doping densities.

Acknowledgements

This work is supported in part by the Air Force Office of Scientific Research (AFOSR) under the award no. FA8650-05-M-2553 and Office of Naval Research (ONR) under award no. N00014-06-1-0227. However, any opinions, findings, conclusions, or recommendations expressed herein are those of the authors and do not necessarily reflect the views of the AFOSR or ONR. Authors would also like to thank Dr. Alan Sugg for the tasks related to the OTPT processing.

References

[1] J.J. Ely, G.L. Fuller, T.W. Shaver, Ultrawideband electromagnetic interference to aircraft radios, in: Proceedings of the Digital Avionics Systems Conference, vol. 2, 2002, pp. 13E4-1–13E4-12.
[2] J.R. Todd, Direct optical control: a lightweight backup consideration, in: Proceedings of the IEEE National Aerospace and Electronics Conference, vol. 2, 1992, pp. 456–463.
[3] http://www.afrlhorizons.com/Briefs/Apr05/VA0412.html.
[4] S.K. Mazumder, T. Sarkar, Optically-triggered power transistor (OTPT) for fly-by-light (FBL) and EMI-susceptible power electronics, Plenary Paper, in: Proceedings of the IEEE Power Electronics Specialists Conference, 2006, pp. 1–8.
[5] S.K. Mazumder, T. Sarkar, Device technologies for photonically-switched power-electronic systems, appeared, in: Proceedings of the IEEE International Pulsed Power Conference, 2005.
[6] S.K. Mazumder, T. Sarkar, M. Dutta, M.S. Mazzola, Photoconductive Devices in Power Electronics, in: Electrical Engineering Handbook, third ed., Taylor & Francis, London, 2006, pp. 9–42.
[7] A. Rosen, F. Zutavern, High Power Optically Activated Solid-State Switches, Artech House, MA, 1994.
[8] C. Furbock, R. Thalhammer, M. Litzenberger, N. Seliger, D. Pogany, E. Gornik, G. Wachutka, A differential backside laserprobing technique for the investigation of the lateral temperature distribution in power devices, in: International Symposium on Power Semiconductor Devices and ICs, 1999, pp. 193–196.
[9] P. Jacob, Defect- and structure-weakness-localization on power semiconductors using OBIRCH (optical beam induced resistivity change), in: Proceedings of the International Symposium on the Physical and Failure Analysis of Integrated Circuits, 2002, pp. 152–156.
[10] T. Yamagata, T. Sakai, K. Sakata, K. Shimomura, High current modulation in optically controlled MOSFET using directly-bonded SiO_2-InP, in: International Topical Meeting on Microwave Photonics, 1996, pp. 173–176.
[11] T. Yamagata, K. Shimomura, High responsivity in integrated optically controlled metal-oxide semiconductor field-effect transistor using directly bonded SiO_2–InP, IEEE Photon. Technol. Lett. 9 (1997) 1143–1145.
[12] A.A.A. De Salles, Optical control of GaAs MESFET's, IEEE Trans. Microwave Theory Tech. 31 (10) (1983) 812–820.
[13] S.B.B. Pal, R.U. Khan, Optically-controlled ion-implanted GaAs MESFET characteristic with opaque gate, IEEE Trans. Electron Devices 45 (1) (1998) 78–84.
[14] P. Chakrabarti, S.K. Shrestha, A. Srivastava, D. Saxena, Switching characteristics of an optically controlled GaAs-MESFET, IEEE Trans. Microwave Theory Tech. 42 (3) (1994) 365–375.
[15] D.M. Kim, S.H. Song, H.J. Kim, K.N. Kang, Electrical characteristics of an optically controlled N-channel AlGaAs/GaAs/InGaAs pseudomorphic HEMT, IEEE Electron Device Lett. 20 (2) (1999) 73–76.
[16] G. Vitale, G. Busatto, G. Ferla, The switching behavior of the bipolar mode field effect transistor (BMFET), in: Proceedings of the IEEE Industry Applications Society Annual Meeting, vol. 1, 1988, pp. 600–605.
[17] G. Breglio, R. Casavola, A. Cutolo, P. Spirito, The bipolar mode field effect transistor (BMFET) as an optically controlled switch: numerical and experimental results, IEEE Trans. Power Electron. 11 (6) (1996) 755–767.
[18] T. Sarkar, S.K. Mazumder, Amplitude, pulse-width, and wavelength modulation of a novel optically-triggered power DMOSFET, in: Proceedings of the IEEE Power Electronics Specialists Conference, 2004, pp. 3004–3008.
[19] M.J. Lazarus, K. Loungis, V.H.W. Allen, Optically controlled high-speed switching of a power transistor, IEEE Trans. Circuits Syst. I 47 (4) (2000) 528–535.
[20] P. Bhadri, D. Sukumaran, K. Ye, S. Dasgupta, E. Guliants, F.R. Beyette Jr., Design of a smart optically controlled high power switch for fly-by-light applications, in: Proceedings of the IEEE Midwest Symposium on Circuits and Systems, vol. 1, 2001, pp. 401–404.
[21] R.P. Zingg, On the specific on-resistance of high-voltage and power devices, IEEE Trans. Electron Devices 51 (3) (2004) 492–499.
[22] G.E. Bulman, V.M. Robbins, K.F. Brennan, K. Hess, G.E. Stillman, Experimental determination of impact ionization coefficients in (1 0 0) GaAs, IEEE Electron Device Lett. 4 (1983) 181–185.
[23] S.M. Sze, Semiconductor Devices: Physics and Technology, Wiley, New York, 2001.
[24] K. Tharmalingam, Optical absorption in the presence of a uniform field, Phys. Rev. 130 (6) (1963) 2204–2206.
[25] M. Brinbaum, T.L. Stocker, Effect of electron–hole recombination processes on semiconductor reflectivity modulation, Br. J. Appl. Phys. 17 (1966) 461–465.
[26] H.R. Philipp, H. Ehrenreich, Optical properties of semiconductors, Phys. Rev. 129 (4) (1963) 1550–1560.
[27] D.E. Aspens, A.A. Studna, Dielectric functions and optical parameters of Si. Ge, GaP, GaSb, GaAs, InP, InAs, and InSb from 1.5 to 6.0 eV, Phys. Rev. B 27 (2) (1983) 985–1009.
[28] R.M. Corless, G.H. Gonnet, D.E.G. Hare, D.J. Jeffrey, D.E. Knuth, On the Lambert *W* function, Adv. Comput. Math. 5 (1) (1996) 329–359.